Chapter 4

Multiple Localized Defect Interaction using Response Surface Methodology

In chapter 3, severity of the fault has been assessed with the help of dynamic modelling, but the interaction between load, speed and defect has not been investigated. This chapter provides insight upon interaction between load and speed in presence of bearing defect of different severity. The presence of the localized defects at the components of the bearing such as at its outer race, inner race and rolling element results into vibration. Monitoring the level of vibration caused by the localized defects, before it reaches to the alarming level, is the important task. Indices of the time domain such as RMS, kurtosis, peak to peak value and crest factor are some of the important parameters for monitoring the condition of rotor bearing system. Localized defect such as spalls of two different sizes on outer and inner race are considered for these studies. Response surface methodology (RSM) as a statistical and mathematical tool is used in this chapter to understand the effect of varying defect size and its interaction with varying rotor speed upon the vibration response, to understand severity of fault. Experimentation are carried out using rotor-bearing test rig and analyzed by using design of experiments. The results from the experimentation are recorded for root mean square (RMS) value of vibration response. RSM has clearly shown the significant change in vibration response due to interaction between factors such as defect size with rotor speed.

4.1 Introduction

The mechanical efficiency and stability of the rotary machine, depends upon the critical component like bearing. A small local fault such as the spall at the components of the bearing such as outer race, inner race and rolling element can lead to vibration in the system and thus becomes one of the major reasons for machine breakdown and catastrophic failure. To ensure the healthy state of rotating machinery, condition monitoring of bearing is highly required in order to avoid breakdown of the system and associated losses to breakdown such as production loss. Therefore, early detection of mechanical fatigue avoids

breakdown. All rotating equipment vibrates to some degree, but as older bearings and components reach the end of their product life, they begin to vibrate more drastically and in distinct ways. Vibration analysis is widely used to detect early indications to machine failure, allowing machinery to be repaired or replaced before an expensive failure occurs. Vibration signals are generated due to the fault in the bearing, these signals contain the information about defective component of bearing. In order to examine the condition of the bearing, variety of the techniques are developed that allows to monitor the occurrence of the defect in the bearings. Vibration signals generated from the defective bearing are analyzed as time domain, frequency domain and time-frequency domain [1,2] (such as wavelet transform, Hilbert transform). The faults of the components of the bearing are classified by using the various artificial intelligence techniques and advanced signal processing (SP) techniques, in order to extract the exact faulty features from the vibration signals and to obtain meaningful data from the results. The various artificial intelligence techniques are ANN (Artificial neural networks) [3,4], SVM (Support vector machine) [5,6] HMM (Hidden Markov Model) [7], genetic algorithm combined with ANN [8]. The simple signal/data processing techniques generally used in many condition monitoring industries are RMS, kurtosis, FFT etc. These simple signal processing (SP) techniques lags in providing the exact faulty information of bearing. Thus, over some past few years, new advanced SP techniques have been developed, such as, wavelet transform, envelope analysis, Hilbert – haung transform, spectral kurtosis, minimum entropy deconvolution (MED) etc. All these techniques are based upon the vibration signals data, which are processed, to detect the fault in the bearing.

Over the years, many researchers, have applied these advanced SP techniques along with artificial intelligent techniques, to obtain the exact fault detection of the bearing. Law et.al [9] presented an approach based upon the wavelet packet transform (WPT) decomposition and Hilbert-haung transform for spindle bearings condition monitoring. Hongyu cui et.al [10] investigated the rolling element bearing for early diagnosis of fault using high frequency characteristics and self-adaptive wavelet de-noising. They located the fault using these techniques with the help of grey correlation method. Manjeevanseera et.al [11] used hybrid intelligent model, FMM-RF, consisted of fuzzy min-max (FMM) neural network and the random forest (RF) for classifying the ball bearing faults. Classification of the fault

in a bearing is most significant task, after obtaining the vibration signals. The vibration signals obtained from the defective bearings are generally the raw signals, which is to be processed with the help of signal processing techniques. The practitioners in the area of condition monitoring, widely used several SP methods to extract the defect features from the raw vibration signals of faulty bearing. There are simple signal processing methods are available which are mainly based upon the statistical parameters such as RMS, mean, kurtosis, crest factor etc. The RMS value have been widely used method which shows the correlation between vibration acceleration and bearing wear over the whole lifetime [12]. T.J Harvey et.al [13] conducted the electrostatic wear monitoring of rolling element bearing to understand its deterioration by considering the RMS value during the experimentation. Similarly, Zhang Zhi-qiang [14], investigated rolling contact fatigue damage using acoustics emission and vibration signals. They have developed the coating of Fe-based alloy using the plasma spraying technology, for investigating fatigue damage of rolling elements. During the experimentation, RMS value provided them clear insight about the damage. Dale W.Schwach and Y.B.Gao[15] conducted the fundamental study to understand the impact of surface integrity by hard turning on rolling contact fatigue. They used acoustic emission (AE) to study the fatigue damage during hard turning. One of the most important AE parameters during their experimentation was RMS, which provided them clear information about fatigue damage. From literature, it is very well proved that RMS plays a significant role in understanding wear and vibration acceleration.

Theoretical judgement based upon the experimental results marks the usefulness of research work. Mathematical tools improve the efficiency of the experiments and provides the meaningful inference from the experimental data. In the present work of research, one such mathematical tool, response surface methodology is used to predict the dynamic response of a rotor bearing system, based upon the experimentation data, obtained from the dedicated rotor-bearing test rig. RSM is a collection of statistical and mathematical techniques useful for developing, improving and optimizing processes [16]. The most important applications of RSM is found in the design, development and formulation of new products as well in improving the existing design of product. M.S.Patil et.al [17] used RSM for condition monitoring of ball bearings. They used RSM to study the influence of defect size, load and speed on the bearing vibrations by using kurtosis as response factor. P.K

kankar et.al [18] performed fault diagnosis of defective rolling element bearing using response surface methodology (RSM). In their work, they developed mathematical formulation to predict discrete spectrum at characteristic defect frequencies and their harmonics. They also performed the experimentation to validate the mathematical results. RSM was used to predict the dynamic response of a rotor bearing system in their research work.

The present study aims in identifying the effect of severity of outer race and inner race defect on the stability and dynamic behavior of rotor bearing system. Therefore, in this work, two different size of defects are artificially seeded upon the surface of the outer race and inner race using electric spark erosion technique. To perform RSM successfully, input and output variables are required. Here size of the defect on outer race and inner race and speed of the rotor are treated as input variables and vibration response in horizontal(X) and Vertical(Z) direction are treated as output variables. Experiments are planned and analyzed using design of experiments (DOE) to study the influence of input variables upon the RMS value. Self-aligned 1204 ball bearing is used for experimentation purpose. The inference is explained in regard to experimental work for this research work.

4.2 Response Surface Methodology

Response surface methodology (RSM) is a collection of statistical and mathematical techniques useful for developing, modelling and analyzing the processes. The significant applications of RSM is in design, development and formulation of new products. In a wide variety of industrial settings such as chemical processes, sheet metal operations, electronic manufacturing, metal cutting and joining processes, RSM has found extensive applications, with the objective of optimizing the responses, particularly when it is potentially influenced by several input variables, which may affect some performance measure or quality characteristic of the product or process. The industrial applications of RSM will have more than one response in many cases. The perspective of the response surface methodology can be clearly understood with the help of graphical representations which is mainly called as response surface plot. In order to understand the relationship between the input variables and responses with the help of graphical representation, contour plot of the response

surface is obtained. The field of response surface methodology consists of the experimental strategy for exploring the space of the process or independent variables (Input variables), empirical statistical modelling to develop an appropriate approximating relationship between the output and the process variables and optimization methods for finding the levels to produce most desirable values of the responses (maximize or minimize). The response of the system is dependent upon the controllable input variables which sometimes called independent variables. If all the input parameters are considered as the quantitative variables, then the responses are the function of input variables.

$$y = f(x_1, x_2, \dots\dots\dots, x_k) + \varepsilon \tag{4.1}$$

Where f is called true response function and ε represents variability sources which is not accounted in f . ε represents the measurement error and various sources of variation associated with the process such as noise.

Here, for an approximation to the true response surface, second order model is used to develop the relationship between the response variable of interest and the input variables which may be described as such

$$y = f(x) = \beta_o + \sum_{j=1}^{k} \beta_j x_j + \sum_{j=1}^{k} \beta_{jj} x_j^2 + \sum_{i<} \sum_{j=2}^{k} \beta_{ij} x_i x_j \tag{4.2}$$

The advantage of using the second -order model in response surface methodology (RSM) is that, it is highly flexible and easy to estimate the parameters (the β's). Such type of the model is known as multiple linear regression model with multiple independent variables. These independent variables may be the predictor variable. Here the parameters β's is called the regression co-efficient and k is the number of factors.

In a multiple linear regression model, the method of least squares is typically used to estimate the regression co-efficient. Therefore, the model in terms of matrix notation may be written as

$$y = X\beta + \varepsilon \tag{4.3}$$

In general y is an n×1 vector of the observations, X is an n×p matrix of the levels of the independent variables, β is a p×1 vector of the regression co-efficient, and ε is a n×1 vector

of random errors. The, matrix B of the regression co-efficient can be obtained as least squares estimator of β as

$$b = (X'X)^{-1}X'y \tag{4.4}$$

The solution to the response surface methodology is obtained in terms of the fitted regression model. Therefore, fitted regression model can be described as

$$\hat{y} = Xb \tag{4.5}$$

In terms of the scalar notation, the fitted regression model can be represented as

$$\hat{y}i = b_0 + \sum_{j=1}^{k} b_j x_{ij} \text{ , } i = 1,2.....n \tag{4.6}$$

After building the empirical model, to measure the usefulness of the model, statistical analysis techniques, such as analysis of variance (ANOVA), is used. This technique is based upon the decomposition of the total variability in the response variable y. The entire process of RSM is shown in Figure 4.2.

4.3 Experimentation

4.3.1 Experimental method.

A bearing fault test rig used for this study is shown in Figure 3.5. Here also the shafts are supported by two 1204 ETN9 self-aligning ball bearing. In these work, separate test bearings are used for experimentation purpose with two different defect sizes on inner race and outer race of bearing. The depth of two sizes of defects used were 0.75 mm and 1.0 mm. The details of fault conditions and defect geometry is given in Table 4.1. These defects which are mainly called as localized defects, have been artificially seeded upon the inner race and outer race component of bearing using spark erosion method. The sample photograph of outer race defect and inner race defect used for this study is as shown in Figure 4.1.

(a)

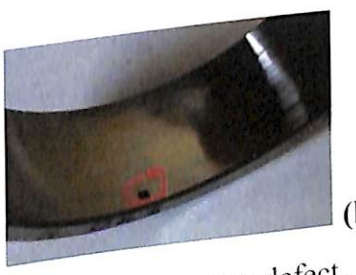

(b)

Figure 4.1 Photograph of defects (a) Inner race defect (b) Outer race defect.

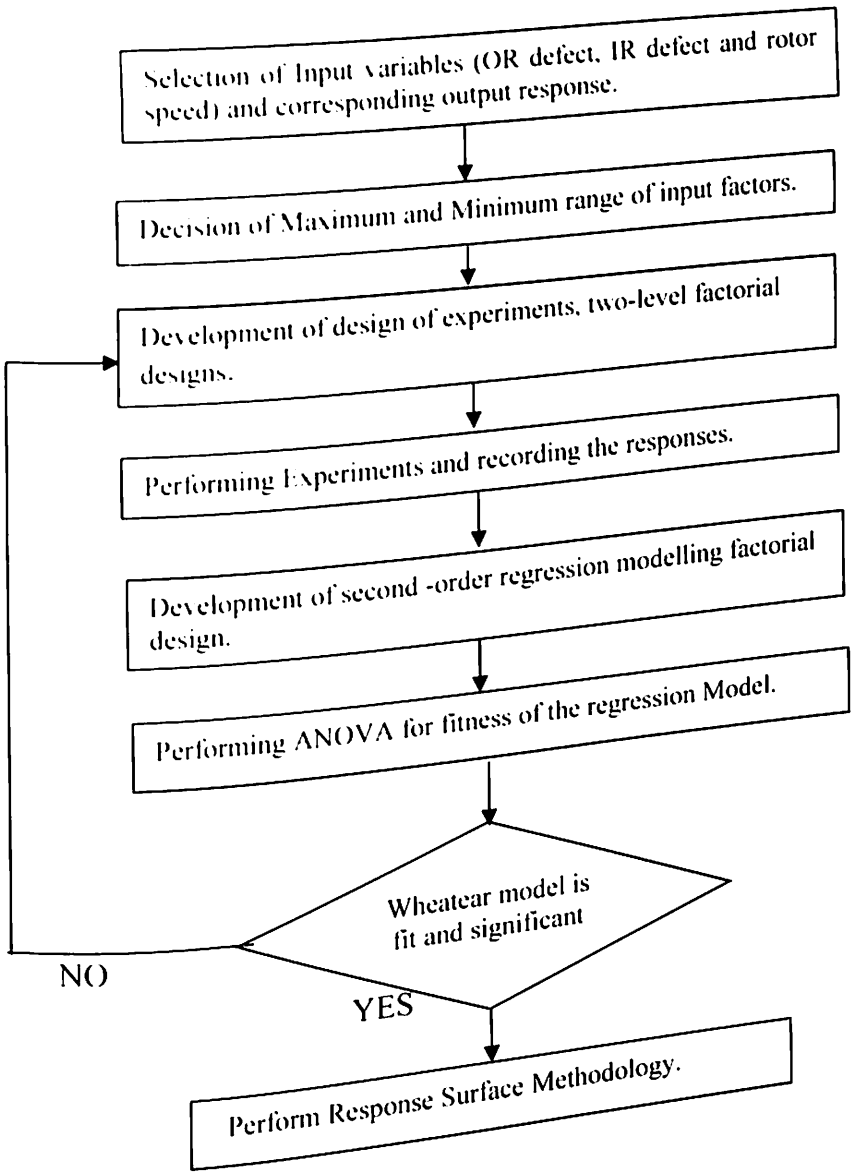

Figure.4.2 Flow Chart for RSM.

In order to obtain the efficient vibration data from the defective bearings of test rig, they are fixed towards the rotor side of the shaft and the other end of the shaft is supported by healthy bearing. At outer race, the localized defect is normally found in loaded region of the bearing, hence for outer race, defect is seeded in a load zone. Bearing loader is used to obtain the radial loading effect. Bearing loader of weight 50 N is used here in a bearing test rig. Arrangement for mounting the accelerometer is made available upon the bearing housing. The accelerometer senses the vibration signals which are generated as the rolling

element traverses through localized defects of outer race and inner race. The tri-accelerometer with the sensitivity of 102.0 mV/g is used for obtaining the vibration signals. The vibration signals are recorded, analysed and filtered using real-time multi-analyser of 8 channels with maximum range of 40 KHZ. Here root mean square (RMS) is considered as the response parameter for vibration response in vertical and horizontal direction. Fast Fourier Transform is used to present the amplitude level of vibration at the characteristic frequency of defect. The experiments are performed into a room temperature and thin layer of lubrication is present upon the races of the bearing.

Table 4.1 Bearing defect size and geometry.

Fault size(mm) (D_{defect})	Location	Defect geometry
0.75	Outer race, Inner race	Rectangular
1.0	Outer race, Inner race	Rectangular

Table 4.2 Parameters for DOE

Parameter Designation Symbol	Parameters	Levels	
		Minimum	Maximum
A	Outer race spall	-1	+1
B	Inner race spall	-1	+1
C	Rotor speed	1500	3000

4.3.2 Design of experiments and factors.

To establish the DOE, three factors of interest as inner race defect, outer race defect and rotor speed are selected with two levels. The minimum and maximum levels are defined in the Table 4.1. In these the reference value for two different size of the defect of the bearing at outer race and inner race component of the bearing is taken as (-1) and (+1). (-1) indicates low severity of fault for fault size 0.75mm and (+1) indicates high severity of fault for fault size 1.0mm, in terms of vibration response. Here the three factors A, B and C, each at two levels are of interest and such a design is called 2^3 factorial design and the eight trail runs which is listed in Table.4.2. The factors A, B and C represents the outer race spall, Inner race spall and rotor speed at its maximum and minimum levels. The + and – signs represents the high and low levels of each factor, which is listed as eight runs in the 2^3 design which is usually called as design matrix shown in Table 4.2. Such a notation is widely used in response surface methodology.

Table 4.3 DOE set and Responses

Run	Factor 1 A (mm)	Factor 2 B (mm)	Factor 3 C (RPM)	Response 1 Horizontal Amplitude (X), RMS, m/s^2	Response 2 Vertical Amplitude (Z), RMS, m/s^2
1	(-1)	(-1)	3000	6.821	15.72
2	(-1)	(+1)	1500	2.423	8.867
3	(+1)	(-1)	1500	2.514	5.062
4	(+1)	(-1)	3000	7.137	14.92
5	(-1)	(+1)	3000	6.402	14.82
6	(+1)	(+1)	1500	2.391	8.84
7	(-1)	(-1)	1500	2.546	5.089
8	(+1)	(+1)	3000	6.725	14.02

Root mean square (RMS) is chosen as the vibration response parameter for both horizontal vibration response and vertical vibration response, as an output parameter required to perform response surface methodology. It is given as

$$\overline{x_{rms}} = \frac{1}{T}\int_0^t \sqrt{x^2(t).dt} \tag{4.7}$$

4.4 Results and Discussion

The design expert statistical package was used to analyze the data obtained from the experimentation and response parameter. The second order polynomials are tested using analysis of variance (ANOVA) at 5% level of significance (95% confidence level) and then RSM of horizontal and vertical vibration responses are developed.

4.4.1 ANOVA for Vibration response in X-direction

In order to check and fit the adequacy of a second order model, obtained from the data resulting from the experimentation, we perform the variance analysis and F-ratio test. The data resulting from the experiments have the two independent variables, Outer race defect and Inner race defect of two different size and two responses, they are, acceleration response in Z-direction i.e vertical acceleration and acceleration response in X-direction i.e horizontal acceleration. Table 4.2. shows the upper and lower levels used for outer race defect and inner race defect in the natural units of measurements. Table 4.3 shows factors with two levels and eight trail runs and recorded vibration responses. Such type of designing the experimental data is called a central composite design and this design is used in this work in order to fit a second order response surface. Table 4.4 shows the analysis of variance for acceleration response in X-direction. Here F value 2.345×10^5 represents that the model is significant. There is only a 0.16% chance that an F-value this large could occur due to noise. Values of "Prob>F" less than 0.0500 indicate model terms are significant. In this case A, B, C, AC, BC are significant model terms. Values greater than 0.1000 indicate the model terms are not significant. If there are many insignificant model terms (not counting those required to support hierarchy), model reduction may improve the present model.

The second order polynomial equation in terms of coded factors for horizontal vibration response is given as

$$X_1 = 2.09 + 0.013 \times A - 0.030 \times B + 0.52 \times C + 3.722 \times 10^{-4} \times AB + 0.018 \times A - 0.010 \times BC \quad (4.8)$$

This second order polynomial equation can be used to make predictions about the horizontal vibration response for given levels of any value of input factors, such as defect size and rotor speed. By default, the high levels of the factors are coded as +1 and low levels of the factors are coded as -1. The coded equation is useful for identifying the relative impact of the factors by comparing the factor co-efficient.

The second order equation in terms of actual factors for horizontal vibration response is given as

$$X_2 = 0.83937 - 0.34804 \times A - 0.014532 \times B + 6.15031 \times 10^{-4} \times C + 0.023818 \times AB + 1.90970 \times 10^{-4} \times AC - 1.08598 \times 10^{-4} \times BC \quad (4.9)$$

The above second-degree polynomial equation can also be used to make predictions about the horizontal vibration response for given levels of any value of input factors, such as defect size and rotor speed. Here, the levels are specified in the original units for each factor. Such equations cannot be used to determine the relative impact of each factor because the co-efficient are scaled to accommodate the units of each factor and the intercept is not at the center of the design space.

4.4.2 ANOVA result for vibration response in Z-direction.

Similar to the ANOVA result for X -direction acceleration response, here also the model value of 228829.06 implies the model is significant. Again, at here also there is only a 0.16% chance that an F-value this large could occur due to noise. Analysis of variance for vibration response in Z- direction is shown in Table 4.5. In this ANOVA, like ANOVA for X-direction, values of "Prob>F" less than 0.500 indicates that model terms are significant. Here A, B, C, AC, BC are the significant model terms. Here, again, values greater than 0.1000 indicate the model terms are not significant.

Here the second order equation in terms of coded factor is given as

$$Z_1 = 3.23 - 0.027 \times A + 0.15 \times B + 0.62 \times C - 2.109 \times 10^{-4} \times AB - 0.025 \times AC - 0.21 \times BC \quad (4.10)$$

The developed equation is useful for predicting the vibration response in Z-direction for any value of input factors such as defect size and rotor speed.

The second order equation in terms of actual factors is given as

$$Z_2 = -4.43047 + 0.38479 \times A + 6.25955 \times B + 3.01577 \times 10^{-3} \times C - 0.013497 \times AB - 2.62694 \times 10^{-4} \times AC - 1.085 - 2.2382 \times 10^{-3} \times BC \quad (4.11)$$

The above equation can also be used to make predictions about the vibration response in Z-direction for any value of input factors such as defect size and rotor speed.

4.4.3 Contour plots

4.4.3.1 Contour plots for Vertical vibration response

Figure 4.3 represents three contour plots for three interaction effect between factors AB, AC and BC at its low level (-1) and high level (+1) upon vertical vibration response. By examining these contour plots for given interactions, it is clear that there is the significant increase in amplitude of vertical vibration response due to varying defect size with varying rotor speed (i.e at low level and high level). The severity of fault can easily be assessed with the increase in vibration level from the fault at 0.75mm to the fault at 1.0 mm of size. with the increase in vibration level from the fault at 0.75mm to the fault at 1.0 mm of size.

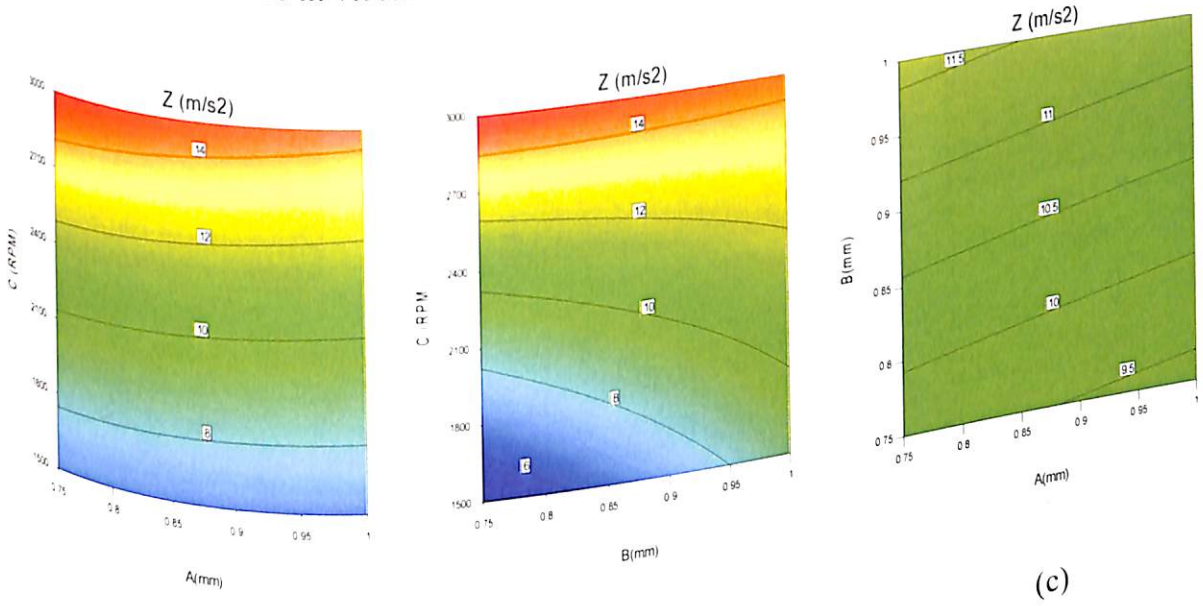

(a) (b) (c)

Figure 4.3 Contour plots for vertical vibration response showing interaction between factors (a) Factor A and B (b) Factor A and C (c) Factor B and C.

4.4.3.2 Contour plots for horizontal vibration response

Figure 4.4 shows the contour plots of three interactions between factors AB, AC and BC. All the three contour plots clearly indicate that, there is a significant change in acceleration response in X-direction, due to the change in defect size and rotor speed at its low and high level. Contour plot of interaction AB is significantly providing the information about the increase in acceleration in X-direction due to the change in defect size at both the inner and outer race of bearing components, at its low and high levels. Contour plots of AC and BC tells us about the effect of change in rotor speed and change in defect size of outer race and inner race upon the acceleration response in X-direction. Investigating these two contour plots clearly indicate, that with the increased speed of rotor, and at high level of defect size, there is an increase in amplitude of vibration response. The increased level of vibration clearly describes the severity of fault.

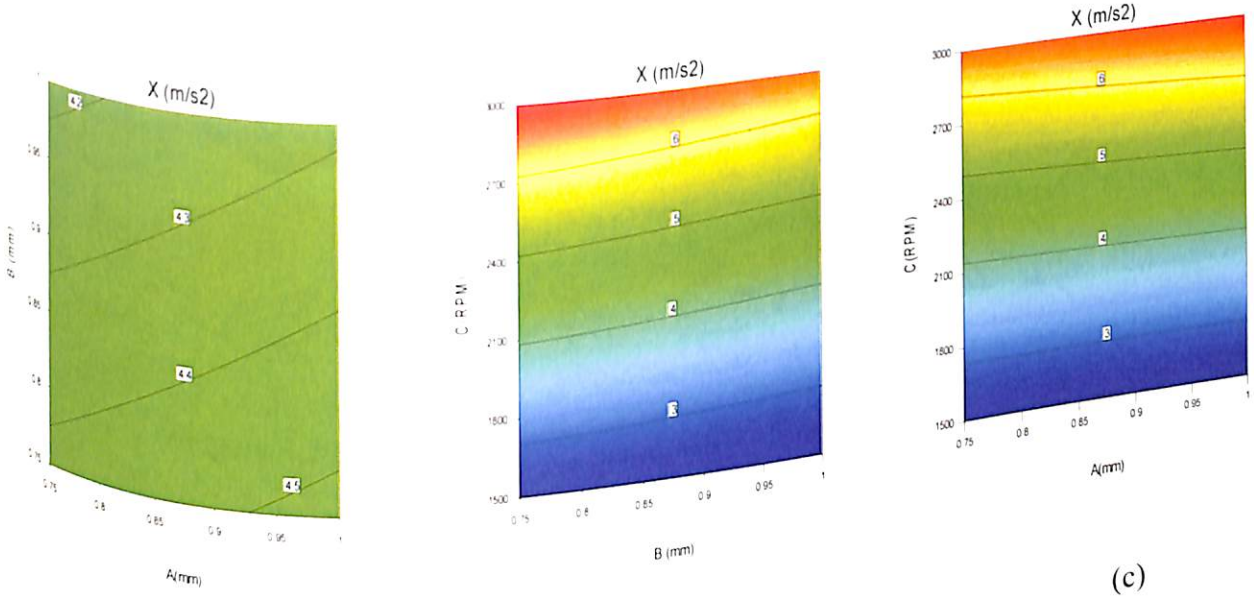

(a) (b) (c)

Figure 4.4 Contour plots for horizontal vibration response showing interaction between factors (a) Factor A and B (b) Factor A and C (c) Factor B and C.

4.4.4 Response Surface plots

4.4.4.1 Response Surface plot for vertical vibration response.

Figure 4.5 represents the response surface plot for all the interactions between factors AB, AC and BC. Response surface plot of AB shows the interaction effect of outer race defect

and inner race defect, whereas response surface plot of AC shows the interaction effect of outer race defect and rotor speed and BC shows the interaction effect of inner race defect and rotor speed, upon the vibration response in Z-direction. Examining the response surface plot of interaction between factors A and B, Figure 4.5(a), provides the clear information about increase in amplitude of vibration due to increase in defect size. However, outer race defect will have more impact upon amplitude of vibration than inner race defect for the same defect sizes. From the response surface plot of interaction between factors A and C (outer race defect and rotor speed), Figure 4.5(b), there is a clear information about increase in the amplitude of vibration at 3000 rpm and 1.0mm of defect size, compared to the amplitude of vibration at 1500 rpm and 0.75 mm of defect size.

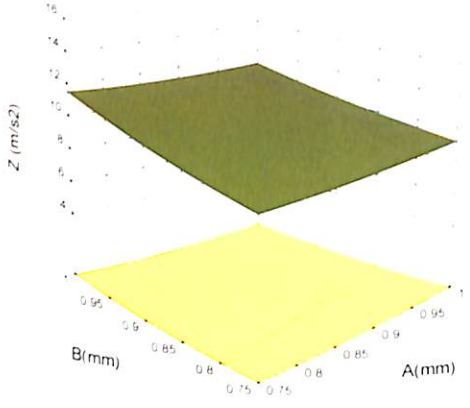

Figure 4.5(a)

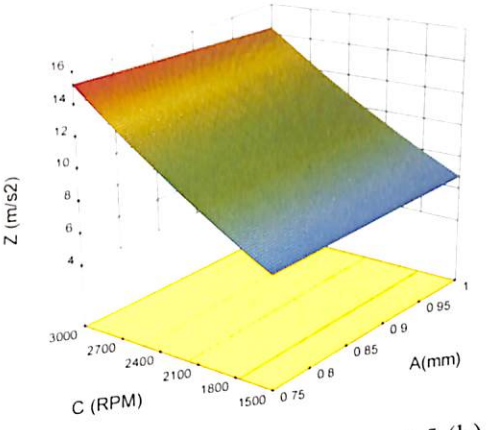

Figure 4.5 (b)

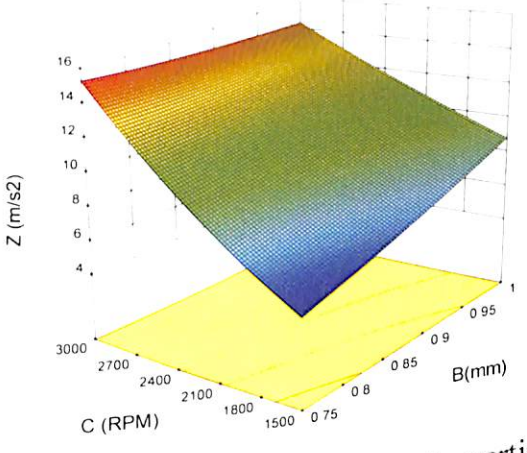

Figure 4.5 (c)

Figure 4.5 RSM plots for vibration response in vertical direction, showing interaction between various factors (a) Factor A and B (b) Factor A and C (c) Factor B and C.

It is clearly visible from the response surface plot, that at high level of defect size in outer race corresponding to high rotor speed leads to maximum level of amplitude of vibration in Z-direction. The response surface plot of interaction between inner race defect and rotor speed (factors B and C) shown in Figure 4.5(c) also reveals the information about increase in amplitude of vibration in Z-direction from low level to high level. However, there is a change into the pattern of response surface plot of outer race defect and inner race defect for same parameters. This is due to the fact that at 3000 rpm the inner race defect on bearing started the catastrophic stage of bearing and due to the self-peening of the bearing defects, amplitude of vibration gets decreased, which is as shown in Figure 4.5(c). The change in vibration response in Z-direction to the outer race defect is more compared to the inner race defect for the same defect size and rotor speed. The performance prediction of predicted vs actual of vibration response in vertical direction is as shown in Figure 4.6. From Figure 4.6, it is clearly shown that actual vs predicted values of response are in close proximity. Hence it verifies the fitness of polynomial for the vertical vibration response.

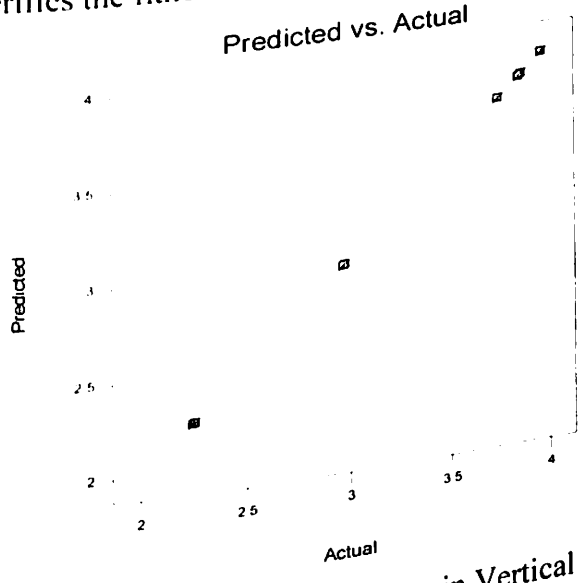

Figure 4.6 Predicted Vs Actual for vibration response in Vertical direction.

4.4.4.2 Response Surface plot for horizontal vibration response

Response surface plots for vibration response in horizontal direction are shown in Figure 4.7. Figure 4.7(a) represents the response surface plot of effect of defect size of inner race and outer race at its low level and high level upon the horizontal vibration response. From the Figure 4.7, it can be seen that at 1.0 mm of defect size of inner race and outer race,

there is an increase in horizontal vibration response due to the outer race defect compared to the inner race defect. The interaction between factors A and B provides the basis for understanding the effect of fault severity upon the vibration response.

Figure 4.7 (b) represents the response surface plot of interaction between two significant factors (A and C), that is outer race defect and rotor speed. The response surface plot represents the effect of interaction between A and C upon the horizontal vibration response. There is a clear indication from the response surface plot that the rotor speed has considerable effect upon the vibration response in the presence of outer race defect.

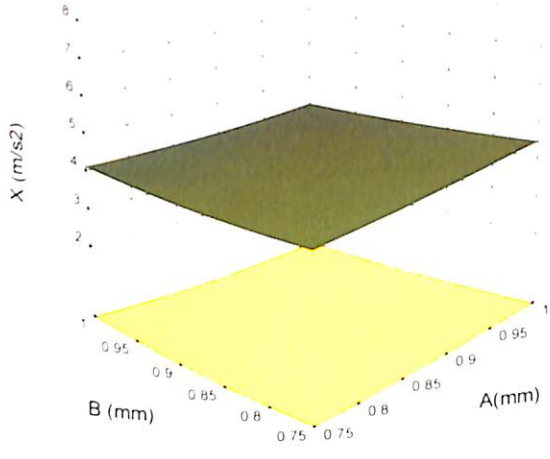

Figure 4.7(a)

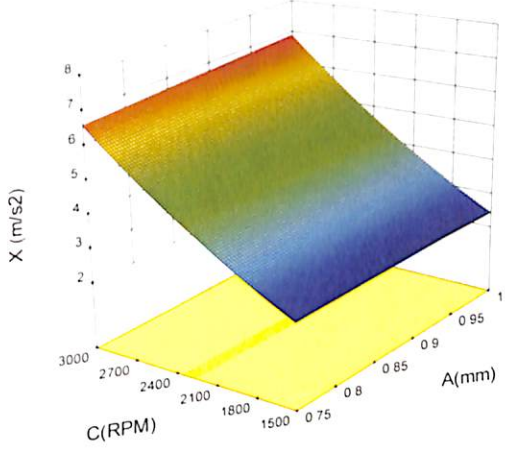

Figure 4.7(b)

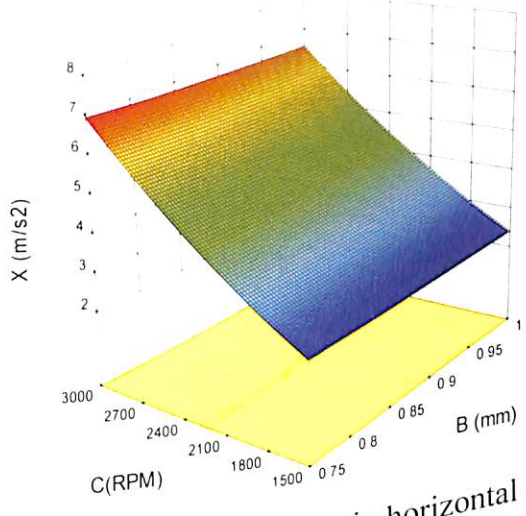

Figure 4.7(c)

Figure 4.7 RSM plots for vibration response in horizontal direction, showing interaction between various factors (a) Factor A and B (b) Factor A and C (c) Factor B and C.

Table 4.4 Analysis of variance table for horizontal vibration response [Partial sum of squares - Type III]

Source	Sum of Squares	Df	Mean Square	F Value	P-value (Prob >F)
Model	2.14	6	0.36	2.345×10^{5}	0.0016
A	$1.313\cdot10^{-3}$	1	1.313×10^{-3}	864.80	0.0216
B	$7.083\cdot10^{-3}$	1	7.083×10^{-3}	4665.52	0.0093
C	2.12	1	2.12	1.399×10^{6}	0.0005
AB	$1.108\cdot10^{-6}$	1	1.108×10^{-6}	0.73	0.5499
AC	$2.564\cdot10^{-3}$	1	2.564×10^{-3}	1689.13	0.0155
BC	$8.292\cdot10^{-4}$	1	8.292×10^{-4}	546.24	0.0272
Residual	$1.518\cdot10^{-6}$	1	1.518×10^{-6}		
Cor Total	2.14	7			

Table 4.5 Analysis of variance table for vertical vibration response [Partial sum of squares - Type III]

Source	Sum of Squares	Df	Mean Square	F Value	P-value (Prob >F)
Model	3.63	6	0.60	2.288×10^{5}	0.0016
A	$5.945\cdot10^{-3}$	1	5.945×10^{-3}	2249.96	0.0134
B	0.18	1	0.18	69461.29	0.0024
C	3.08	1	3.08	1.166×10^{6}	0.0006
AB	3.558×10^{-7}	1	3.558×10^{-7}	0.13	0.7761
AC	4.852×10^{-3}	1	4.852×10^{-3}	1836.40	0.0149
BC	0.35	1	0.35	1.333×10^{5}	0.0017
Residual	2.642×10^{-6}	1	2.642×10^{-6}		
Cor Total	3.63	7			

The increase in rotor speed with maximum size of defect has increased level of vibration. The level of vibration amplitude has shown the considerable increase due to change in rotor speed from 1500 rpm to 3000 rpm, with change in defect size from 0.75mm to 1.0 mm.

This indicates the effect of severity of fault upon the change in vibration level. Figure 4.7(c) represents the response surface plot of interaction between factors B and C (inner race defect and rotor speed) upon the horizontal vibration response.

Here also, change in rotor speed with change in defect size from minimum level to maximum level has shown the considerable effect upon the horizontal vibration response. However, compared to Figure 4.7(b), outer race defect has more impact upon the vibration response than inner race defect for the same rotor speed.

The performance prediction of predicted vs actual of vibration response in horizontal direction is as shown in Figure 4.8. Here also, from Figure 4.8, it is clearly shown that actual vs predicted values are in close proximity. Hence it verifies the fitness of polynomial for horizontal vibration response.

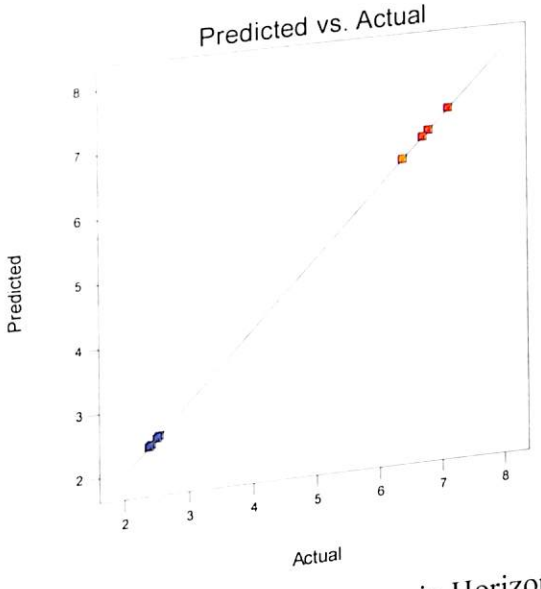

Figure 4.8 Predicted Vs Actual for vibration response in Horizontal direction.

4.4.5 Interaction Plot

4.4.5.1 Interaction plot for Vertical vibration response.

Figure 4.9 shows the interaction plot for interaction of factors. The two-factor interaction shown in Figure 4.9 is helpful in the practical interpretation of the results.

The interaction between the factors A&B is shown in Figure 4.9 (a), which is the interaction between the two-defect size of outer race defect and inner race defect. Here, the line with square end points represents the low-level effect and line with triangle end points represent the high-level effect upon the acceleration response in Z direction.

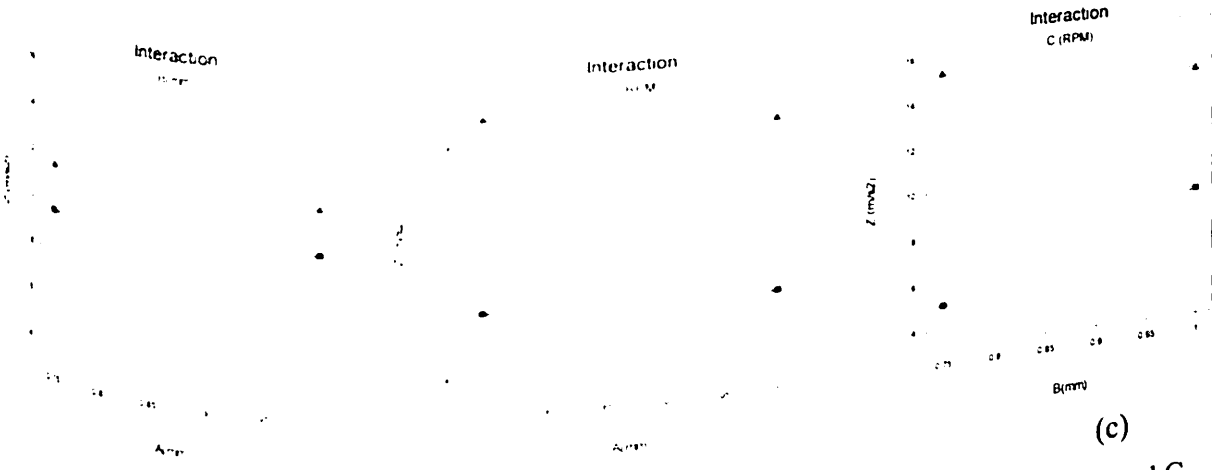

(a) (b) (c)

Figure 4.9 Interaction plot (a) Factor A and B (b) Factor A and C (c) Factor B and C.

Similarly, Figure 4.9(b) show the interaction graph of two factors A & C, which is the interaction between outer race defect and rotor speed at its low and high level, upon the acceleration response in Z direction. The interaction plot between these two factors has shown a significant effect upon the acceleration response in Z-direction. From the interaction plot, it clearly shows, that at low level rotor speed there is a small change in acceleration response due to change in defect size at outer race component of bearing, but at high level of rotor speed, significant change in acceleration response is observed due to the change in defect size at outer race at its low and high level. The investigation of these interaction plot clearly indicates that outer race defect has significant impact upon acceleration response in Z-direction due to high level rotor speed. The interaction plot of factors B and C is shown in Figure 4.9(c), which is the interaction plot between the inner race defect and rotor speed at its low level and high level. From the interaction plot, it is very clear that the inner race defect has much more impact upon the acceleration response in Z-direction compared to the impact caused by outer race defect. Investigating, the interaction plot, provides the information about the significant increase in amplitude at high level defect size of inner race and low-level rotor speed, compared to high level defect size

and rotor speed. This effect is similar to outer race defect for same combination of levels. The amplitude of vibration is decreasing at high level of defect size and rotor speed, due to the "self-peening" of the bearing defect.

4.4.5.2 Interaction plot for horizontal vibration response.

The interaction plot between factors A&B is shown in Figure 4.10(a). From the plot, it clearly indicates that, there is an increase in amplitude level of vibration due to change in defect size from its low level to high level. Similarly, the interaction plot between the factors A&C is shown in Figure 4.10(b). Here, it shows the effect of interaction between the outer race defect and rotor speed at its low and high level upon the acceleration response in X-direction. Figure 4.10(b), clearly indicates that, there is no significant change in amplitude response at low level of interaction factors, but at high level of interaction factors, the increase in amplitude level of vibration has been very well observed. Figure 4.10(c) shows the interaction plot of factors B and C, which is the interaction plot of inner race defect and rotor speed at its low level and high level. The Fig indicates that there is the decrease in amplitude level of vibration response in X-direction at low level of input factors, whereas there is an increase in amplitude level of vibration response in X-direction at high level of input factors.

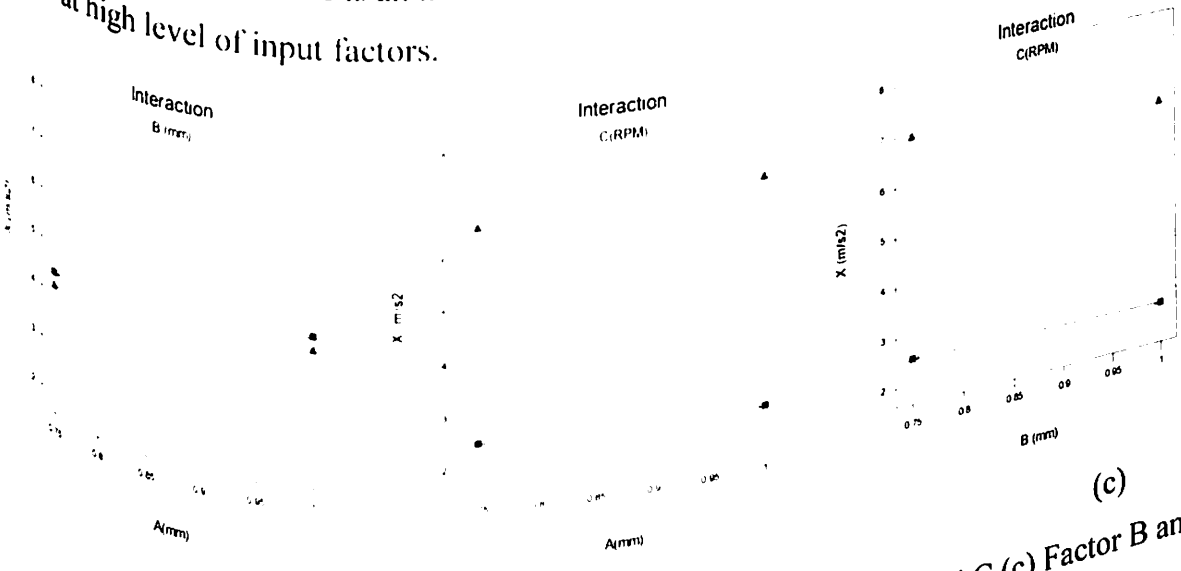

(a) (b) (c)

Figure 4.10 Interaction plot (a) Factor A and B (b) Factor A and C (c) Factor B and C.

4.5 Conclusion

In the present experimental investigation, to study the effect of input variables upon the acceleration response in vertical and horizontal direction of self-aligning rolling element bearing, response surface methodology is used. Localized defect of two different sizes are introduced upon the outer race and inner race component of bearing. These defect of two different sizes, along with change in rotor speed are considered as input variables to study the change in response due to the effect of interaction between input factors as well as individual effect of factor. DOE is used to conduct the trail experimentation. Eight no. of trial experimentation are carried out and vibration responses in horizontal and vertical direction are recorded. ANOVA is used for the vibration responses in both the direction to test the significance of regression model. The results of the ANOVA for both the vibration responses positively tested the significance of model and thus second -order polynomial multiple regression model was significantly fitted for all its interaction factor as well as individual factors for both the responses. Response surface plots, contour plots and interaction plots are developed to determine the effect of change in defect size with change in rotor speed at its high and low level upon the acceleration response in both the directions. The severity of fault assessment is carried out with the help of all plots. These plots provided the clear view of change in vibration response due to the interaction effect of factors as well as individual effect of factors at its low and high level. Some of the important conclusions drawn, from the obtained responses are

1] For the same input factors, outer race defect shows the large impact upon the vibration response in vertical direction than the vibration response in horizontal direction.

2] In the case of outer race defect, at the high-level rotor speed, the vibration response in Z-direction increases first at low level defect size and then decreases at high level defect size. However, the vibration response in X-direction decreases first at low level and then increases at high level of defect size.

3] In the case of inner race defect, at low level of rotor speed, there is no significant change in amplitude of vibration response in X-direction at low and high level of defect size. However, outer race defect shows the significant increase in amplitude of vibration response from low level to high level of defect size.

The next chapter describes about expert system of fault diagnosis. The present chapter tells us only about interaction effects, but classification of faults is considered to be important aspect of fault diagnosis.

References

1] D. F. Shi, W. J. Wang, and L. S. Qu, (2004). "Defect Detection for Bearings Using Envelope Spectra of Wavelet Transform," J. Vib. Acoust., vol. 126, no. 4, p. 567.

2] H. Cao, F. Fan, K. Zhou, and Z. He, (2016). "Wheel bearing fault diagnosis of trains using empirical wavelet transform," Meas. J. Int. Meas.Confed., vol. 82, pp. 439–449.

3] B. SAMANTA and K. R. AL-BALUSHI, (2003) ."Artificial Neural Network Based Fault Diagnostics of Rolling Element Bearings Using Time-Domain Features," Mech. Syst. Signal Process., vol. 17, no. 2, pp. 317–328,.

4] M. Unal, M. Onat, M. Demetgul, and H. Kucuk, (2014). "Fault diagnosis of rolling bearings using a genetic algorithm optimized neural network," Measurement, vol. 58, pp. 187–196.

5] A. Widodo and B.-S. Yang, (2007). "Support vector machine in machine condition monitoring and fault diagnosis," Mech. Syst. Signal Process., vol. 21, no. 6, pp. 2560–2574,.

6] A. Rojas and A. K. Nandi, (2006) "Practical scheme for fast detection and classification of rolling-element bearing faults using support vector machines," Mech.Syst Signal Process., vol. 20, no. 7, pp. 1523–1536,.

7] H. Ocak and K. A. Loparo, (2005) "HMM-Based Fault Detection and Diagnosis Scheme for Rolling Element Bearings," J. Vib. Acoust., vol. 127, no. 4, p. 299.

8] J. Chen and R. B. Randall, (2016) "Intelligent diagnosis of bearing knock faults in internal combustion engines using vibration simulation," Mech. Mach. Theory, vol. 104, pp. 161–176,.

9] L. S. Law, J. H. Kim, W. Y. H. Liew, and S. K. Lee, (2012) "An approach based on wavelet packet decomposition and Hilbert Huang transform (WPD-HHT) for spindle bearings condition monitoring," Mech. Syst. Signal Process.,vol. 33, pp. 197–211,.

10] H. Cui, Y. Qiao, Y. Yin, and M. Hong, (2015) "An investigation of rolling bearing early diagnosis based on high-frequency characteristics and self-adaptive wavelet de-noising," Neurocomputing, vol. 216, pp. 649–656,.

11] M. Seera, M. L. D. Wong, and A. K. Nandi, (2017) "Classification of ball bearing faults using a hybrid intelligent model," Appl. Soft Comput. J., vol. 57, pp. 427–435,.

12] I. El-thalji and E. Jantunen, (2015) "A summary of fault modelling and predictive health monitoring of rolling element bearings," Mech. Syst. Signal Process., vol. 60–61, pp. 252–272,.

13] T. J. Harvey, R. J. K. Wood, and H. E. G. Powrie, (2007) "Electrostatic wear monitoring of rolling element bearings," Wear, vol. 263, no. 7–12 SPEC. ISS., pp. 1492–1501,.

14] Z. Q. Zhang, G. L. Li, H. D. Wang, B. S. Xu, Z. Y. Piao, and L. N. Zhu, (2012) "Investigation of rolling contact fatigue damage process of the coating by acoustics emission and vibration signals," Tribol. Int., vol. 47, pp. 25–31,.

15] D. W. Schwach and Y. B. Guo, (2006) "A fundamental study on the impact of surface integrity by hard turning on rolling contact fatigue," Int. J. Fatigue, vol. 28, no. 12, pp. 1838–1844,.

16] Mayers R H and Montgomery D C, Response surface Methodology: Process and product optimization using designed experiments, 4th ed, Wiley, New York. 2000

17] M. S. Patil, J. Mathew, P. K. Rajendrakumar, and S. Karade, (2010) "Experimental Studies Using Response Surface Methodology for Condition Monitoring of Ball Bearings," J. Tribol., vol. 132, no. 4, pp. 44505,.

18] P. K. Kankar, S. C. Sharma, and S. P.Harsha, (2011) "Fault Diagnosis of High Speed RollingElement Bearings Due to Localized Defects Using Response Surface Method," J. Dyn. Syst. Meas. Control, vol. 133, no. 3, pp. 31007.